

Multiple-order Raman scattering in crystalline and amorphous silicon

A. Zwick and R. Carles

Laboratoire de Physique des Solides, Université Paul Sabatier, 118 route de Narbonne, 31062 Toulouse CEDEX, France

(Received 5 January 1993; revised manuscript received 26 April 1993)

Raman-scattering measurements have been performed on *c*-Si and *a*-Si over a wide range of frequencies, including Stokes and anti-Stokes sides, and up to fourth order. All the features are accounted for by using the same physical parameters in both phases. In particular, it is shown that multiple-order scattering processes are not negligible, but rather of the same order of magnitude as first-order processes. In amorphous materials, light-scattering excess, spurious background, Boson-peak or hot-luminescence processes, which have been recently put forward, turn out to be mainly caused by high-order Raman-scattering processes.

I. INTRODUCTION

The simplest way to describe the structure of an amorphous material like *a*-Si consists of considering that short-range coordination is preserved whereas the extended atomic network is random.¹ In other words, this means that the local coordination is tetrahedral (sp^3 hybridization) as in crystalline Si (*c*-Si); the values of the first-nearest-neighbor distance, coordination number, or binding energy remaining more or less the same in the amorphous and crystalline phases.

Also, the covalent nature of the bonds means that short-range interactions play a preeminent role. Hence it is not surprising that the energy spectra of the density of electronic or vibrational states are similar in amorphous Si (*a*-Si) and *c*-Si.² For example, the semiconducting properties are preserved in *a*-Si, and the density of vibrational states (DVS) reflects a smoothed version of the crystalline DVS.³ As a matter of fact, the greatest differences are induced by the presence of dangling bonds. In practice, however, this can be circumvented by sample hydrogenation of the amorphous material, since hydrogen is a good terminator for insaturated bonds. From the theoretical point of view,² it has often been shown that the main features of the density of states can be accounted for by a molecular description (tight-binding or valence-force-field models). The effect of the topological disorder mainly consists of a broadening of these features.

This work concerns coupling between the corresponding excitations (electron-phonon interaction). Raman spectra in *c*-Si and *a*-Si are compared over a wide spectral range, namely in the anti-Stokes and Stokes parts, and up to the fourth order. It is demonstrated that the second- and higher-order effects are not negligible and that the overall scattering efficiency is similar in both materials.

The paper is organized as follows. Following this brief introduction, Raman data are first presented and discussed in Sec. II for *c*-Si, and the variation of the total scattering efficiency versus the scattering order is addressed. Then in Sec. III, Raman results are given and reviewed for hydrogenated *a*-Si. Finally, in Sec. IV, the

accuracy of the proposed model is assessed and the validity of most of the previous scattering analysis on highly disordered materials is questioned.

II. RAMAN SCATTERING IN *c*-Si

Prior to analyzing the Raman effect in *a*-Si, the impact on *c*-Si must be reconsidered. Indeed, although often researched, this issue contains some areas, often overlooked, which turn out to be particularly important for achieving a precise interpretation of the Raman effect in disordered materials.

A. Experimental results

Figure 1(a) shows the Raman spectrum recorded in backscattering geometry from a (111)-oriented single crystal of undoped Si. This record was obtained at room temperature using the 488-nm line of an Ar⁺ laser as the exciting light. This wavelength was selected because (i) the setup response is roughly frequency independent in most of the spectral range investigated, and it remains unchanged irrespective of the polarization of the scattered field relative to the gratings; (ii) the resonance will slightly distort the spectrum since the corresponding energy is far from the main electronic transitions in Si. Scattered light was dispersed through a triple monochromator and detected by a low-noise photomultiplier. To minimize sample heating, the laser beam was focused through a cylindrical lens. Importantly, only the dark noise of the detector (which is obviously frequency independent) has been subtracted from the rough spectra.

B. Spectrum interpretation

Most of the features depicted in Fig. 1(a) have already been reported.⁴ The first-order Raman spectrum consists of the two strong peaks located at $\pm 520 \text{ cm}^{-1}$ (+ for Stokes, - for anti-Stokes) and ascribed to the creation (+) or annihilation (-) of the triply degenerated long-wavelength optical phonons $0(\Gamma)$.

The second-order spectrum is composed of much weaker structures (about two orders of magnitude less)

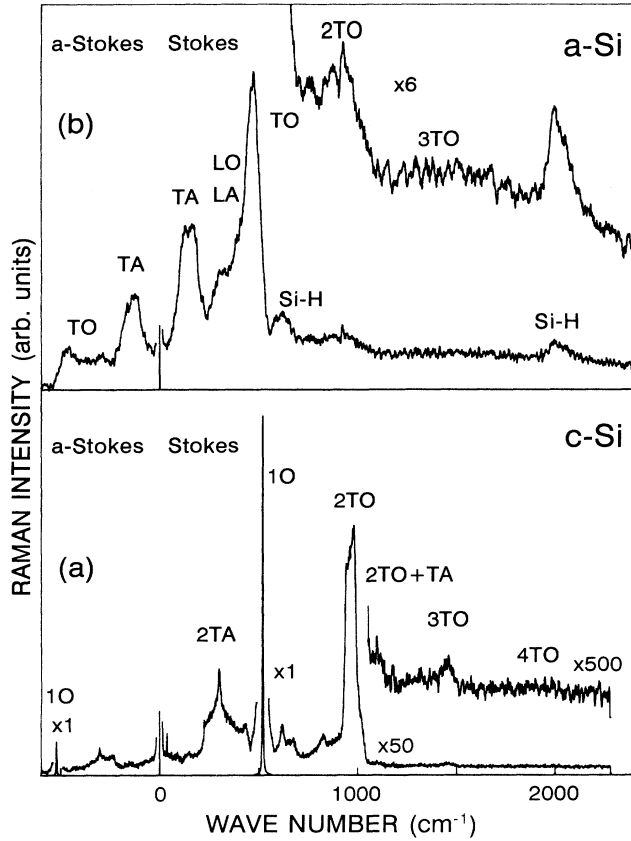


FIG. 1. Experimental Stokes and anti-Stokes Raman spectra of (a) (111) crystalline silicon and (b) hydrogenated amorphous silicon, obtained with the 488 nm exciting line at room temperature.

spread over the 0–1040 cm^{-1} range on the Stokes side. It has been observed that the overtone scattering belonging to the totally symmetric Γ_1 component dominates the second-order Raman spectrum in all tetrahedrally bonded semiconductors.⁵ Figure 1(a) also shows that the anti-Stokes scattering rapidly vanishes when the frequency shift $|\omega|$ increases, according to population factor effects (see below).

Moreover, Fig. 1(a) shows third-order Raman features: the 1400–1960- cm^{-1} band is ascribed to 3TO scattering⁶ and the 1040–1150 cm^{-1} to 2TO+TA. These multiple-order effects are more clearly evidenced in Fig. 2(a), where the second-, third-, and fourth-order spectra are reported on scales multiplied by 2, 3, and 4, respectively: The overtones are thus superimposed. In particular, with an amplification factor of 8000, 4 TO processes can be originally highlighted as shown in Fig. 2(a).

C. Differential cross sections and population effects

Due to the wave vector selection rule and the low value of incident and scattered wave vectors (\mathbf{k}_i and \mathbf{k}_s , respectively), it is well known that only the long-wavelength modulation of polarizability is efficient in a Raman pro-

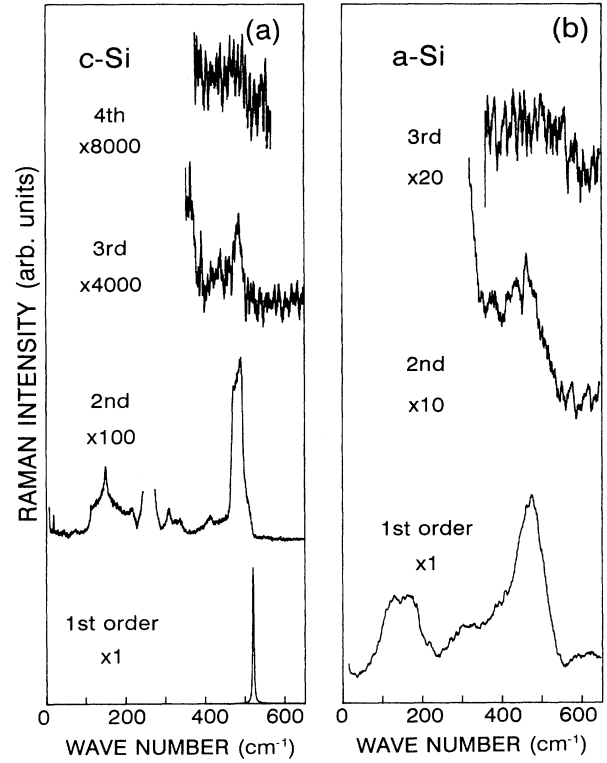


FIG. 2. Multiple-order Raman scattering in (a) c-Si and (b) a-Si. Frequency scales have been multiplied by the scattering order.

cess, namely

$$\mathbf{k}_i - \mathbf{k}_s = \mathbf{k}_{\text{diff}} \cong \mathbf{0}. \quad (1)$$

In a crystalline material, each eigen vibrational mode (i.e., each phonon) labeled m_p is characterized by its wave vector \mathbf{q}_p , energy $\hbar\omega_p$, and eigenvector symmetry Γ_p . This set of characteristics is simply denoted $\{m_p\}$.

Generalizing the expression for second-order Raman scattering,⁷ the differential cross section for n -order Raman scattering can then be written as

$$\frac{d^2\sigma^{(n)}}{d\Omega d\omega} = A \sum_{\{m_p\}} C_{\{m_p\}} \left[\prod_{p=1}^n \frac{\bar{n}_p + 1}{\omega_p} \right] \times \delta \left[\mathbf{k}_{\text{diff}} - \sum_{p=1}^n \mathbf{q}_p \right] \delta \left[\omega - \sum_{p=1}^n \omega_p \right], \quad (2)$$

where the summation is restricted to sets $\{m_p\}$ whose frequencies satisfy the energy conservation law

$$\omega_i - \omega_s = \omega = \sum_{p=1}^n \omega_p \quad (3)$$

and whose wave vectors satisfy the quasimomentum conservation law

$$\sum_{p=1}^n \mathbf{q}_p = \mathbf{k}_{\text{diff}} \cong \mathbf{0}. \quad (4)$$

The coefficient $C_{\{m_p\}}$ accounts for the Raman selection rule reflecting the electron- $(n$ -phonon) interaction. Then it depends on the wave-vector value and the symmetry of the n phonons involved.

In Eq. (2), \bar{n} is the temperature-dependent Bose-Einstein factor which verifies the useful relation

$$\frac{\bar{n}(-\omega)+1}{(-\omega)} = \frac{\bar{n}(\omega)}{\omega} \quad (5)$$

Note in particular that in Eqs. (2) and (3) the value of ω is either positive (Stokes side) or negative (anti-Stokes side). In these relations the value of ω_p is likewise positive (creation) or negative (annihilation), and thus in Eq. (2) all the n -order processes (additive, subtractive, combinations and overtones) are taken into account with the appropriate population factors.

Parameter A depends on the optical properties of the sample and accounts for the ω^4 scattering law. In this study, the selected exciting wavelength and the small variation of both optical properties and scattering frequency ω_s allows us to disregard its variation versus ω . Indeed, the experimental variation of parameter A does not exceed a few percent and is therefore below the experimental uncertainties.

In addition, the ratio of the total Stokes scattering efficiency I_S versus the anti-Stokes I_{aS} at a given Raman shift $\omega > 0$ is given by

$$\frac{I_S}{I_{aS}} = \exp(\beta\hbar\omega) \quad (6)$$

Worthy of note is the fact that this relation originates from general thermodynamic considerations⁸ and is therefore independent of the harmonic approximation and scattering order.

The differential cross section for second-order Raman scattering is given by⁷

$$\frac{d^2\sigma^{(2)}}{d\Omega d\omega} = A \sum_{m_1, m_2} C_{m_1, m_2} \frac{\bar{n}_1 + 1}{\omega_1} \frac{\bar{n}_2 + 1}{\omega_2} \times \delta(\mathbf{k}_{\text{diff}} - \mathbf{q}_1 - \mathbf{q}_2) \delta(\omega - \omega_1 - \omega_2) \quad (7)$$

Following Eq. (4), the summation is restricted to phonons belonging to the same point in the reduced Brillouin zone ($\mathbf{q}_1 = -\mathbf{q}_2$). As already mentioned, and contrary to previous work,⁷ this equation can be applied to describe either additive or subtractive modes, either Stokes or anti-Stokes scattering.

In fact, since most of the spectrum features are ascribed to overtones, one obtains

$$\frac{d^2\sigma^{(2)}}{d\Omega d\omega} = A \sum_m C_{m, m} \left[\frac{\bar{n}_m + 1}{\omega_m} \right]^2 \delta(\omega - 2\omega_m) \quad (8)$$

If it is roughly assumed that the whole factor of the δ function under the summation sign does not depend on the mode, it follows that

$$\frac{d^2\sigma^{(2)}}{d\Omega d\omega} \propto \sum_m \delta(\omega - 2\omega_m) = g_c \left(\frac{\omega}{2} \right), \quad (9)$$

where $g_c(\omega)$ is the one-phonon density of states in c -Si.

Figure 3(a) depicts the one-phonon density of states calculated by Weber⁹ using a bond-charge model. Figure 3(b) shows the comparison between the second-order Raman spectrum and the DVS with a frequency scale obviously multiplied by 2. The whole second-order spectrum is remarkably well described. Certain slight discrepancies on the high-frequency tail of the first-order line are due to combination bands.⁴ In addition, the experimental data exhibit a continuous scattering excess which underlies the whole second-order spectrum [see dotted line in Fig. 3(b)].

Figures 4(a) and 4(b) depict the first-order range experimental intensity on the Stokes (0 and 600 cm^{-1}) and anti-Stokes sides (-600 and 0 cm^{-1}). The anti-Stokes scattering efficiency σ_{aS} can be derived from that of Stokes σ_S , following Eq. (6). Indeed, this can be checked experimentally, as shown in Fig. 4(f), and yields an excellent result using $T = 320$ K and taking into consideration the whole signal at a given frequency. In other words, the continuous "background" underlying the first- and second-order features is due primarily to inelastic light scattering. This aspect has been always ignored. The present data clearly show that the true background level (i.e., dark noise of the photomultiplier) is effectively

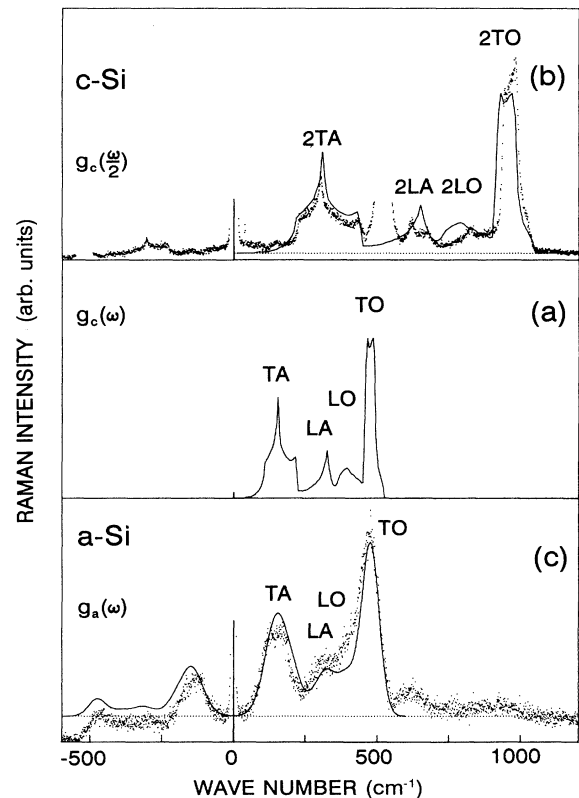


FIG. 3. (a) Density of vibrational states $g_c(\omega)$ of c -Si from Weber (Ref. 9). (b) Second-order Raman spectrum of c -Si (dots) compared on the Stokes side with $g_c(\omega/2)$. (c) Raman spectrum of a -Si (dots) compared with $g_c(\omega)$ convoluted by a Gaussian function.

reached at high anti-Stokes wave numbers, when inelastic light scattering is negligible ($\omega < -600 \text{ cm}^{-1}$). Hence the structureless "background" signal can be regarded as the signature of multiple-order Raman processes: It will therefore be governed by relation (6). The identity between spectra (a) and (f) in Fig. 4 is effectively observed for the first-order peak or the 2TA band. Moreover, in the very low-frequency range, the signal (hatched area) follows relation (6) and is therefore also ascribed to Raman-scattering processes.

From Eq. (6), one can define a reduced scattering efficiency I_R as follows:

$$\frac{I_S}{\bar{n}+1} = \frac{I_{aS}}{\bar{n}} = I_R. \quad (10)$$

I_R can also be derived experimentally from the following relation:

$$I_S - I_{aS} = I_R. \quad (11)$$

These two equations support three distinct methods of determination of I_R . The corresponding checks are reported in Figs. 4(c)–4(e): Again the similarity between the spectra is obvious. Unlike the first check [Figs. 4(a), 4(b), and 4(f)], the reduced intensity I_R vanishes at $\omega=0$ due to the exponential variation of the Bose-Einstein factor \bar{n} .

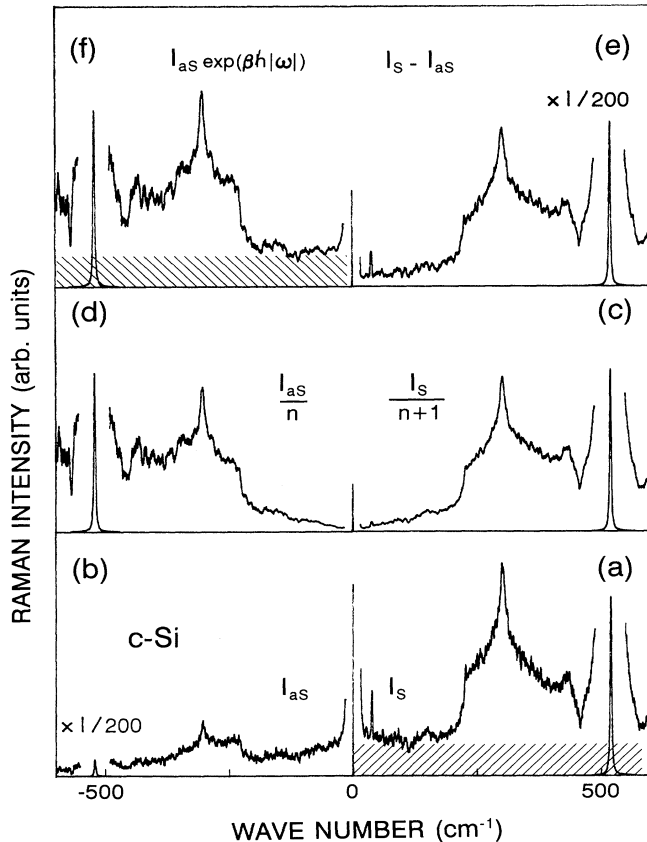


FIG. 4. Low-frequency Raman spectrum of *c*-Si. (a) Experimental Stokes spectrum. (b) Experimental anti-Stokes spectrum. (c)–(f) Reduced spectra.

D. Second- and higher-order scattering efficiencies

It is often claimed that the second-order Raman efficiency is very low relative to the first order. In fact, this is only supported by the scaling change between the corresponding two spectra. Indeed, in Fig. 2, the second-order spectrum has been multiplied by 100. Nevertheless, due to the q -selection rule (4), the first-order signal originates only from the intense peaks located at $\pm(520 \pm 2) \text{ cm}^{-1}$, whereas the second order spans from -1040 to $+1040 \text{ cm}^{-1}$. Thus the corresponding integrated scattering cross sections were evaluated as

$$\frac{d\sigma^{(i)}}{d\Omega} = \int_0^\infty \frac{d^2\sigma^{(i)}}{d\Omega d\omega} d\omega', \quad i=1 \text{ or } 2. \quad (12)$$

As we are only interested in the ratio $\alpha_{2/1}$ of these cross sections, the ω_s dependence of factor A in Eqs. (2) and (7) is discarded. Also, a deconvolution of the rough spectra is not needed to take into account the response function of the experimental setup, since it can be easily demonstrated that at constant resolution the two integrated signals are equally affected.

From the present data derived at $T=320 \text{ K}$, with $E_i=2.54 \text{ eV}$, we obtained $\alpha_{2/1}=0.34$. This value indicates that the Raman-scattering cross section is only divided by 3 when going from first- to second-order Raman scattering in this single crystal.

With the help of the same procedure, the relative contribution of high-order processes was also evaluated. In spite of larger uncertainties, one gets $\alpha_{(n>2)/1} \cong 0.3$.

The present analysis of the Raman effect in *c*-Si has shown exhaustively the advantage of considering both types of scattering (anti-Stokes and Stokes). In addition it has highlighted the relative importance of multiple-order scattering. The latter point is in fact corroborated by the high value of deformation potentials corresponding to electron-two-phonon processes in this type of compounds.⁵

III. RAMAN SCATTERING IN *a*-Si:H

A. Experimental results

In order to compare the Raman effect in *a*-Si and *c*-Si, the spectrum obtained from *a*-Si:H film was recorded under the same experimental conditions as before. The film was grown using chemical-vapor deposition. A great deal of work has already focused on the variation of the Raman spectra (line-shape analysis) versus the growth parameters.^{10,11} However, in this work we do not discuss the growth procedure since we are primarily concerned with the general trends of the phenomena. The sample was only selected on account of its amorphous nature. Additionally, the presence of hydrogen allows the effect of dangling bonds and/or microvoids to be limited. From the lattice dynamics point of view, the presence of hydrogen manifests itself through bond-bending and bond-stretching vibrations of Si-H_n entities that are easily identified.¹²

The Raman spectrum from -600 to 2500 cm^{-1} is reported in Fig. 1(b). Again only the dark noise of the pho-

tomultiplier has been subtracted. The spectrum shape is characteristic of a highly disordered solid material: As a whole, it is composed of broad bands. Two preeminent structures merge and are ascribed to first-order scattering by vibrational modes^{3,10-12} which correspond to TA (50–200 cm^{-1}) and TO (440–520 cm^{-1}) phonons in *c*-Si. The shoulder on the low-energy tail of the TO band (250–440 cm^{-1}) has been ascribed to LA- and LO-like modes. All these first-order structures are also visible on the anti-Stokes side with a lower intensity due to population factor effects [see Eq. (6)].

Figure 1(b) shows the Si-H bond-stretching band located at 2000 cm^{-1} and the corresponding bond bending or wagging around 640 cm^{-1} .¹² In addition, second-order features can also be observed, particularly the 2TO centered at 960 cm^{-1} . Not so easily noticed is the presence of the 2LA (Ref. 13) and TO+TA,¹² since their contribution is partially hidden by the Si-H band.

Of particular relevance in the interpretation of any Raman experimental data is how to make sure that a recorded signal truly accounts for a Raman process. For example, the background signal which underlies the Stokes spectrum in *a*-Si has often been ignored and arbitrarily subtracted because of its “unknown origin (Rayleigh),”¹¹ or interpreted in terms of a “boson peak like in glasses”¹⁴ or “hot luminescence.”¹⁵ Using the same procedure as in

c-Si, and according to Eqs. (5), (10), and (11) and Fig. 4, Fig. 5 depicts the experimental and reduced spectra of *a*-Si. First, the anti-Stokes spectrum multiplied by $\exp(\beta\hbar|\omega|)$ is compared in Fig. 5(f) to the Stokes spectrum [Fig. 5(a)]. As a whole, the reported signal follows relation (5), particularly the continuous signal [hatched areas in Figs. 5(a) and 5(f)]: It must therefore be considered as a Raman process. To ascertain this, we compare the reduced spectra I_R calculated using relations (10) and (11): The difference between Stokes and anti-Stokes spectra is reported in Fig. 5(e). Stokes and anti-Stokes spectra divided by $|\bar{n}+1|$ are reported in Figs. 5(c) and 5(d), respectively. Again the similarity between the three signals is obvious.

These checks assume a particular importance when one endeavors to discriminate between a Raman process, a luminescence process, or an “unknown background.” Also, the procedure used in Figs. 4(e) and 5(e) allows the temperature-dependent population factor effect to be deleted without any temperature knowledge: This is a definite advantage when the temperature of the sample zone investigated by the Raman probe is not known, as is often the case.

B. Multiple-order scattering

The second-order Raman spectrum of *c*-Si [Fig. 1(a)] exhibits a 2TA band (220–460 cm^{-1}) whose maximum intensity is only twice smaller than the 2TO band. The same is expected in the amorphous state if the modification is due only to the lack of geometrical order. Then the 2TA band is blended with the first-order LA- and LO-like bands (200–480 cm^{-1}) and therefore not easily identified. This is probably why second-order effects have often been neglected.¹⁶

The very low-frequency part of the spectrum consists of an intense signal which rapidly decreases relative to the Raman shift $|\omega|$. This “Rayleigh wing” has been interpreted as spurious scattering^{10,11} or light-scattering excess.^{17,18} However, Fig. 5 shows that in *a*-Si it does result from Raman scattering. Since second-order effects are not negligible, a low-frequency modulation of the electronic polarizability by all the differential combination modes is expected. To ascertain this, we have verified that the corresponding band rapidly decreases when the temperature is lowered, in accordance with population factor effects.¹⁹

On the other hand, the present data (Fig. 2) highlight third-order Raman scattering in *a*-Si: Despite a very low-scattering efficiency, the broad band between 1200 and 1700 cm^{-1} is ascribed to 3TO-like modes. Indeed, both its maximum position and shape can be accounted for by multiplying by 3 the frequency scale of the 1TO-like band. Finally, all these findings support the view that most of the observed “background” in hydrogenated amorphous silicon is brought about by multiple-order processes. Since the density of states in the amorphous state has lost all the sharp singularities indicative of long-range correlation in *c*-Si, the Raman bands are spread over wide frequency domains.

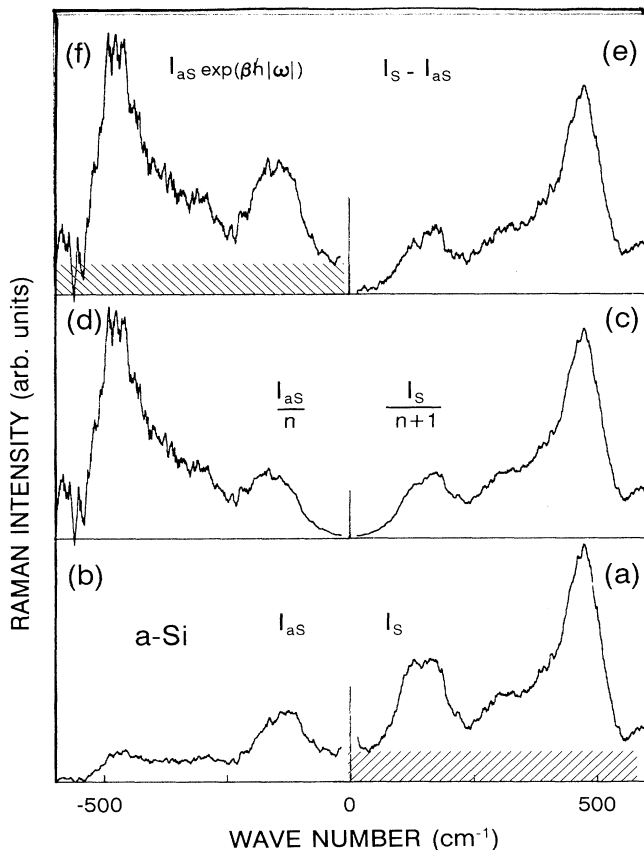


FIG. 5. Low-frequency Raman spectrum of *a*-Si: (a) Experimental Stokes spectrum. (b) Experimental anti-Stokes spectrum. (c)–(f) Reduced spectra.

IV. MODEL FOR LIGHT SCATTERING IN AMORPHOUS MATERIALS

A. The proposed model

Since short-range order and short-range interactions are thought to be essentially the same in the crystalline and amorphous states, these two systems approximately present the same energetic density of vibrational states (DVS). The lack of translational invariance only blurs the long-range correlation effects. For *a*-Si, the validity of these two assertions has been tested either theoretically^{20,21} or experimentally through Raman-scattering,³ infrared-absorption,²² or neutron-scattering²³ data. The experimental results are well accounted for by a local description of the lattice dynamics and the coupling between vibrational modes and the probe (bond polarizabilities, local charge transfer, bond-length and bond-angle distortions . . .). In addition, these local approaches succeed not only for *a*-Si but also for *c*-Si.^{9,24,25}

Our interpretation of the Raman-scattering data in amorphous silicon follows the same approach: (i) lattice dynamics is primarily the same in *c*-Si and *a*-Si due to the same local order and the homopolar nature of the bonds; (ii) the local distortions of bonds only affect the Van Hove singularities of DVS; (iii) the lack of long-range order invalidates all **q**-selection effects; and (iv) the interaction between light and vibrational excitations is governed in both *c*-Si and *a*-Si by the same bond polarizability parameters.

B. Lattice dynamics in *a*-Si

Different attempts have been made to calculate the DVS $g_a(\omega)$ in *a*-Si.² The most reliable ones have been based on a realistic description of the structure and first-principles calculations. Phenomenological approaches rely on the modification of DVS in *c*-Si induced by the geometrical disorder. In all cases the accuracy of the models is discussed by comparing the results with infrared-absorption, neutron-diffraction, neutron-scattering, or Raman-scattering data. Unfortunately, these verifications are disturbed by coupling matrix-element effects which significantly affect the spectra. Also, harmonic approximation is generally used and multiple order mechanisms disregarded.

Hence the use of the simplest DVS determination which consists of convoluting the crystal DVS $g_c(\omega)$ by a normalized Gaussian function $G(\omega, \Gamma)$:³

$$g_a(\omega) = \sum_m \delta(\omega - \omega_m) = g_c(\omega) * G(\omega, \Gamma). \quad (13)$$

The broadening parameter Γ accounts for the reduction of the coherence length of the phonons, induced by the structural disorder. Although convolution broadens the bands and removes the Van Hove singularities of the crystal DVS, it preserves the type of modes (TA, LA, LO, and TO) and their relative contribution.

C. First-order Raman scattering

The differential first-order Raman-scattering efficiency is derived from Eq. (2), in which n equals 1 and the **q** selection rule is omitted. Hence,

$$\frac{d^2\sigma^{(1)}}{d\Omega d\omega} = A \frac{\bar{n} + 1}{\omega} \sum_m C_m \delta(\omega - \omega_m). \quad (14)$$

This analytical relation shows the effect of the coupling-matrix element C_m . In their highly accurate work, Shuker and Gammon²⁶ assumed that this element remained constant for each band from which mode m originates. In more recent works,^{16,27} C_m was taken to be independent of the eigenvector of mode m and chosen as a monotonic function of ω_m . Based on this assumption, one obtains

$$\frac{d^2\sigma^{(1)}}{d\Omega d\omega} = A \frac{\bar{n}(\omega, T) + 1}{\omega} C(\omega) g_a(\omega). \quad (15)$$

In Fig. 3(c), the calculated DVS $g_a(\omega)$ is directly compared to the experimental Stokes spectrum. Following Eq. (13), convolution was performed using $\Gamma = 25 \text{ cm}^{-1}$ and the phonon density of states g_c [Fig. 3(a)] calculated by Weber.⁹ In all previous works, an arbitrary background was subtracted from the experimental spectrum to verify: $I(\omega=0)=0$ and $I(\omega > \omega_{\text{TO}})=0$. Following such a procedure [see dotted line in Fig. 3(c)], the overall data trend is well accounted for, particularly the relative heights of the TA- and TO-like bands. Hence the experimental features are well accounted for, except for the “background.”

Some comments have to be made. Slight discrepancies still remain in the line shapes. Particularly remarkable are the sharp cutoffs of the TA- and TO-like bands in the experimental spectrum. Indeed, the convolution procedure (13) has likewise blurred all DVS singularities. Importantly, the preservation of these sharp discontinuities in the disordered material DVS is equally observed in the neutron-scattering data.²³ These observations support the computational effort required to obtain realistic models of the amorphous structure dynamics: As a matter of fact, the spectra thus derived better reflect such discontinuities.^{20,21}

The agreement between calculated and first-order experimental spectra implies that the coupling matrix element $C(\omega)$ follows rather well the relation

$$C(\omega) \frac{\bar{n} + 1}{\omega} = \text{const}. \quad (16)$$

From this experimental result, for $\omega > 0$ one derives

$$C(\omega) \propto \frac{\omega}{\bar{n}(\omega, T) + 1} = \omega \left[1 - \exp \left[-\frac{\omega}{\omega_0} \right] \right]. \quad (17)$$

In the low-frequency range ($\omega \ll \omega_0$), Eq. (17) becomes

$$C(\omega) \propto \omega^2 \quad (18)$$

Thus the expected squared frequency variation of the coupling factor for Debye phonons, which has already been verified experimentally²⁸ for $20 < \omega < 65 \text{ cm}^{-1}$, is

recovered. In the high-frequency range ($\omega \gg \omega_0$), relation (17) yields $C(\omega)\alpha\omega$. For $T=320$ K, the calculation gives $\omega_0 \cong 200$ cm.⁻¹ Indeed, this critical value roughly coincides with the gap between acoustical and optical phonons in Si, more precisely between propagative and nonpropagative modes. The coupling factor is therefore different for high-frequency modes corresponding to optical and zone-edge acoustical phonons in *c*-Si. For these, the Einstein approximation or a molecular description would be more appropriate. Many attempts have been made to calculate the frequency dependence of the coupling factor. Numerous semiempirical relations have been obtained and consistently predict a slower variation than in the low-frequency range. More significant are the experimental measurements of $C(\omega)$ in *a*-Si,²⁹ which can well be accounted for by Eq. (17). Our assumption is thus supported both theoretically and experimentally.

Equation (15) includes both Stokes ($\omega > 0$) and anti-Stokes ($\omega < 0$) processes by defining $g_a(-\omega) = g_a(\omega)$ and taking into account the identity of the matrix element in both processes: $C(-\omega) = C(\omega)$. Using this equation, the anti-Stokes part of the spectrum has been calculated and is depicted in Fig. 3(c). The relative intensities of the two main bands are well reproduced. However, the subtraction of a constant background is now in total discrepancy with the experimental result. As already mentioned, higher-order effects have to be considered.

D. Second- and higher-order processes

Omitting the wave-vector selection rule in relation (7), and therefore allowing all combinations of vibrational modes, the second-order Raman-scattering cross section for Stokes and anti-Stokes processes is written as follows:

$$\frac{d^2\sigma^{(2)}}{d\Omega d\omega} = A \sum_{m_1, m_2} C_{m_1, m_2} \frac{\bar{n}_1 + 1}{\omega_1} \frac{\bar{n}_2 + 1}{\omega_2} \delta(\omega - \omega_1 - \omega_2). \quad (19)$$

The density of two-phonon states including all the combinations, additive or subtractive (ω_1 and ω_2 being either positive or negative), can be written as

$$g^{(2)}(\omega) = \sum_{m_1, m_2} \delta(\omega - \omega_1 - \omega_2). \quad (20)$$

Again, relation (19) shows that the Raman cross section is not proportional to the density of states, due to the effect of the coupling matrix element C_{m_1, m_2} but mainly to population factor effects. In other words, the variation of the second-order spectrum versus temperature or the ratio between two different structures must be analyzed using relation (19). To our knowledge, this area has always been neglected.

Neglecting selective resonance effects, the coupling between electrons and modes m_1 and m_2 may be regarded as depending only on their frequencies ω_1 and ω_2 . This dependence will be rather monotonic and similar to that observed for overtone scattering in *c*-Si. However, the coefficient C_{m_1, m_2} vanishes for $|\omega| \rightarrow 0$ as a result of

translational invariance of the electronic susceptibility.⁵ The following analytical expression can therefore be formulated:

$$C_{m_1, m_2} = C'(\omega_1)C'(\omega_2), \quad (21)$$

and one gets

$$\frac{d^2\sigma^{(2)}}{d\Omega d\omega} = A \left[\sum_{m_1} C'_1 \frac{\bar{n}_1 + 1}{\omega_1} \delta(\omega - \omega_1) \right] * \left[\sum_{m_2} C'_2 \frac{\bar{n}_2 + 1}{\omega_2} \delta(\omega - \omega_2) \right]. \quad (22)$$

Hence the second-order spectrum can be viewed as an autoconvolution of a one-order spectrum. The latter reflects true one order if C' presents the same frequency dependence as the first-order coupling matrix element C [see Eqs. (15), (17), and (18)]. As they are smoothly frequency-dependent, this simplification can be made. Finally, using Eqs. (15) and (16), one obtains

$$\frac{d^2\sigma^{(2)}}{d\Omega d\omega} \propto \left[\frac{d^2\sigma^{(1)}}{d\Omega d\omega} \right]^{*2}, \quad (23)$$

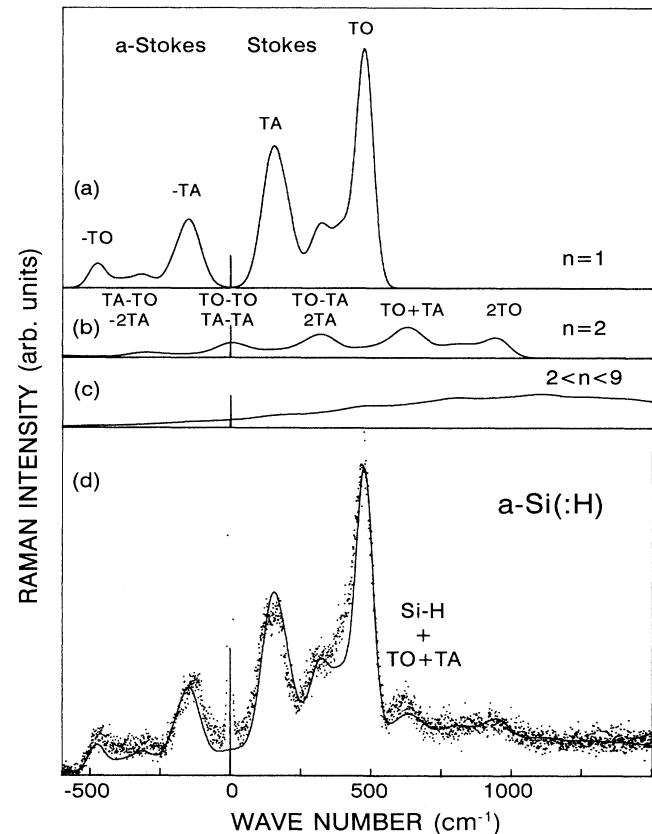


FIG. 6. Calculated Raman spectra of *a*-Si. (a) First order. (b) Second order. (c) Higher orders. (d) Comparison between the experimental (dots) and theoretical (continuous line) spectra.

where superscript $*2$ stands for the autoconvolution product.

It is then straightforward to demonstrate that the n -order scattering efficiency can be written as

$$\frac{d^2\sigma^{(n)}}{d\Omega d\omega} \alpha \left[\frac{d^2\sigma^{(1)}}{d\Omega d\omega} \right]^{*n} \quad (24)$$

Finally, the total Raman spectrum results from the summation of all the different orders, namely

$$\frac{d^2\sigma}{d\Omega d\omega} = \sum_{n=1}^{\infty} \alpha_{n/1} \frac{d^2\sigma^{(n)}}{d\Omega d\omega} \quad (25)$$

Coefficient $\alpha_{n/1}$ accounts for the decrease with n of the scattering efficiency and $\alpha_{1/1}$ equals 1.

E. Comparison with the experimental result

Figure 6(a) depicts the first-order spectrum ($n=1$) using Eqs. (15) and (16). Figure 6(b) depicts the second-order spectrum ($n=2$) using Eq. (23). The autoconvolution was performed in the $[-1200-$ and $+1200\text{-cm}^{-1}]$ frequency range in order to describe all the combination processes. The assignments of the main bands are reported in Fig. 6(b). Of particular relevance is the appearance of a band centered at 0 cm^{-1} which accounts for the vibrational difference processes. The scaling factor $\alpha_{2/1}$ has been chosen equal to that derived from the analysis of the Raman data in c -Si: $\alpha_{2/1}=0.34$. The greatest part of the experimental spectrum is well accounted for with first and second order only. The choice of the weighting factors for $n > 2$ [Fig. 6(c)] is not of prime importance as they represent only the slightly increasing remaining background: A single value $\alpha_{n/1}=0.17$ was used for all orders. Following Eq. (26), the resulting calculated spec-

trum is calculated and then compared with the experimental one in Fig. 6(d). On the whole, the Raman spectrum is very well fitted. Indeed, all the features are represented, that is, either their frequency location or their relative intensities. No questionable "background subtraction" procedure is used. The low-frequency signal is ascribed to subtractive combinations scattering and the total recorded signal follows relation (6).

V. CONCLUSION

Raman scattering in c -Si and a -Si has been interpreted over a very wide range of frequencies. In this paper, it has been demonstrated that this scattering cannot be correctly described without taking into account anti-Stokes and multiple-order scattering processes. In both a -Si and c -Si, these processes lead to a contribution of the integrated cross section which is of the same order of magnitude as first-order processes. The lack of translational invariance from the crystalline phase to the amorphous one can be accounted for by simply removing the corresponding Raman selection rules.

In our model, the same parameters have been used in both phases. In other words, the bond polarizabilities and the potential anharmonicity are virtually the same. In a local description, this result can be regarded as the persistence of the chemical coordination, and the covalent nature of bonding. In this sense, efforts have to be made to improve the accuracy of the theoretical descriptions of Raman scattering in highly disordered materials.

ACKNOWLEDGMENTS

The Laboratoire de Physique des Solides is Unité de Recherche Associée au CNRS No. 74.

¹D. E. Polk, *J. Non-Cryst. Solids* **5**, 365 (1971).

²For a review, see, for example, B. Kramer and D. Weaire, in *Amorphous Semiconductors*, edited by M. H. Brodsky, Topics in Applied Physics Vol. 36 (Springer-Verlag, Berlin, 1979), p. 9; S. R. Elliot, *Physics of Amorphous Materials* (Longman Inc., New York, 1983); N. E. Cusack, in *The Physics of Structurally Disordered Matter*, edited by Douglas F. Brewer (Bristol, Philadelphia, 1987).

³J. E. Smith, Jr., M. H. Brodsky, B. L. Crowder, M. I. Nathan, and A. Pinczuk, *Phys. Rev. Lett.* **30**, 1141 (1973).

⁴P. A. Temple and C. E. Hathaway, *Phys. Rev. B* **7**, 3685 (1973).

⁵M. Cardona, in *Light Scattering in Solids II*, edited by M. Cardona and G. Güntherodt, Topics in Applied Physics Vol. 50 (Springer-Verlag, Berlin, 1982), p. 19.

⁶P. B. Klein, Jin Joo Song, and R. K. Chang, in *Proceedings of the Third International Conference on Light Scattering in Solids*, edited by M. Balkanski, R. C. C. Leite, and S. P. S. Porto (Flammarion, Paris, 1975), p. 93.

⁷J. S. Lannin and P. J. Carroll, *Philos. Mag.* **B 45**, 155 (1982).

⁸L. Landau and E. Lifchitz, in *Electrodynamics* (Mir, Moscow, 1969), p. 493.

⁹W. Weber, *Phys. Rev. B* **15**, 4789 (1977).

¹⁰D. Bermejo and M. Cardona, *J. Non-Cryst. Solids* **32**, 405 (1979).

¹¹J. S. Lannin, L. J. Pilione, S. T. Kshirsagar, R. Messier, and R. C. Ross, *Phys. Rev. B* **26**, 3506 (1982).

¹²M. H. Brodsky, M. Cardona, and J. J. Cuomo, *Phys. Rev. B* **16**, 3556 (1977).

¹³D. Bermejo, M. Cardona, and M. H. Brodsky, in *Amorphous and Liquid Semiconductors* (University of Edinburgh, Edinburgh, 1977), p. 343.

¹⁴M. Ivanda, K. Furic, O. Gamulin, and D. Gracin, *J. Non-Cryst. Solids* **137 & 138**, 103 (1991).

¹⁵I. H. Campbell, P. M. Fauchet, S. A. Lyon, and R. J. Nemanich, *Phys. Rev. B* **41**, 9871 (1990).

¹⁶C. Thomsen and A. Bustarret, *J. Non-Cryst. Solids* **141**, 265 (1992).

¹⁷G. Winterling, *Phys. Rev. B* **12**, 2432 (1975).

¹⁸R. J. Nemanich, *Phys. Rev. B* **16**, 1655 (1977).

¹⁹A. Zwick *et al.* (unpublished).

²⁰A. Alben, D. Weaire, J. E. Smith, and M. H. Brodsky, *Phys. Rev. B* **11**, 2271 (1975).

²¹K. Winer and M. Cardona, *Solid State Commun.* **60**, 207 (1986).

²²S. C. Shen, C. J. Fang, M. Cardona, and L. Genzel, *Phys. Rev. B* **22**, 2913 (1980).

²³W. A. Kamatikahara, H. R. Shanks, J. F. McClelland, U. Buchenau, F. Gompf, and L. Pintschovius, *Phys. Rev. Lett.*

- 52, 644 (1984).
- ²⁴K. Winer and M. Cardona, *Phys. Rev. B* **35**, 8189 (1987).
- ²⁵S. Go, H. Bilz, and M. Cardona, *Phys. Rev. Lett.* **34**, 580 (1975).
- ²⁶R. Shuker and R. W. Gammon, *Phys. Rev. Lett.* **25**, 222 (1970).
- ²⁷R. Carles, A. Zwick, M. A. Renucci, and J. B. Renucci, *Solid State Commun.* **41**, 557 (1982).
- ²⁸J. S. Lannin, *Solid State Commun.* **12**, 947 (1973).
- ²⁹Fang Li and J. S. Lannin, *Phys. Rev. B* **39**, 6220 (1989).